ASCE
American Society of Civil Engineers

December 2007
Volume 133, Number 12

ISSN 1090-0241
CODEN: JGGEFK

Journal of Geotechnical and Geoenvironmental Engineering

contents continue on back cover

GEO INSTITUTE
The Geo-Institute

Support Mechanisms of Rammed Aggregate Piers. II: Numerical Analyses

Ha T. V. Pham, A.M.ASCE[1]; and David J. White, A.M.ASCE[2]

Abstract: This paper is the second of a two-part series describing an investigation of the mechanical behavior of rammed aggregate piers in supporting rigid square footings. In this paper, the performances of two pier-supported footings and three isolated piers during compressive load tests were simulated using an axisymmetric finite element model and compared to experimental data. A hardening-soil constitutive model with parameters estimated from in situ and laboratory tests was used to characterize the constitutive behaviors of the pier material and the matrix soil. Pier groups were modeled as unit cells with the tributary area determined from the center-to-center spacing. Cavity expansion modeling was used to simulate the pier installation process. Verifications of the numerical model were carried out by comparing the numerical results with the data obtained from full-scale, instrumented load tests. Interpretation of the numerical results focused on the load-deformation behavior, group effect, stress concentration ratio, and the development of stresses in the matrix soil. The distributions of vertical stress underneath the pier-supported footings are also characterized.

DOI: 10.1061/(ASCE)1090-0241(2007)133:12(1512)

CE Database subject headings: Finite element method; Piers; Settlement; Stress concentration; Stress distribution; Numerical analysis.

Introduction

The use of rammed aggregate piers (RAPs) to reduce excessive settlement of column footings constructed over soft soils has been well documented (Lawton and Fox 1994; Lawton et al. 1994; Wissmann et al. 2001). It was reported by Lawton and Fox (1994) that settlements observed at a number of structures stabilized by RAPs were generally less than those predicted using conventional geotechnical procedures for settlement analysis. Similar observations were later reported by Lawton et al. (1994), Handy et al. (1999), and Wissmann et al. (2001). The discrepancy between the predicted and the actual settlement is believed to be a result of (1) the conservatism of the stiffness-based approach used to calculate the upper-zone settlement; (2) the omission of the increase in confinement in the pier-reinforced zone achieved from pier installation; (3) the omission of the pier-soil-pier interactions within the pier group; (4) the limitations of the predicted stress distributions underneath the pier-supported footing; and (5) the difficulties in predicting the compressibility of the soil below the pier group.

Part I of this two-part series (White et al. 2007) describes the experimental results of full-scale load tests on two trial pier-supported footings and three isolated RAPs when subjected to compressive loads. Part II of this series herein presents a numerical study in which the pier-supported footings and isolated RAPs are simulated through the use of an axisymmetric finite element (FE) model. The construction-induced stress regime in the pier-reinforced zone was regenerated by considering pier installation as a cavity expansion process (Pham et al., private communication, 2005). Constitutive modeling parameters of the compacted aggregate and the matrix soils were estimated from the results of in situ and laboratory tests (White et al. 2002; 2003). In this study, a pier-supported footing is modeled as a unit cell. The stress distributions in the upper and the lower zone are characterized based on numerical results.

Numerical Modeling

Constitutive Model

The hardening-soil model developed by Schanz et al. (1999) was used to describe the constitutive behaviors of the matrix soils and the aggregate in this study. The hardening-soil model is essentially a nonlinear, elastoplastic model in which the yield surface in the principal stress space consists of a hardening hexagonal yield surface enclosed by a hardening cap. Failure of the material is defined in accordance with the Mohr-Coulomb criterion. Nonassociated flow rule is used to determine plastic strains on the yield surface whereas associated flow rule is used to characterize plastic straining on the cap. Constitutive model parameters of the hardening-soil model can be readily determined from consolidated drained triaxial and one-dimensional consolidation tests (Schanz et al. 1999). Constitutive model parameters of the desiccated fill layer were assumed based on the data from in situ tests (see White et al. 2007). Table 1 summarizes the values of the constitutive parameters used for the matrix soils and the aggregate. Complete details of the constitutive behaviors of the compacted aggregate and the matrix soils are presented in Pham (2005).

[1]Geotechnical Engineer, CH2M Hill, 1100 112th Ave., Suite 400, Bellevue, WA 98004-4504. E-mail: ha.pham@ch2m.com

[2]Associate Professor, Dept. of Civil, Construction and Environmental Engineering, Iowa State Univ. of Science and Technology, Ames, IA 50011-3232. E-mail: djwhite@iastate.edu

Note. Discussion open until May 1, 2008. Separate discussions must be submitted for individual papers. To extend the closing date by one month, a written request must be filed with the ASCE Managing Editor. The manuscript for this paper was submitted for review and possible publication on December 13, 2005; approved on January 6, 2007. This paper is part of the *Journal of Geotechnical and Geoenvironmental Engineering*, Vol. 133, No. 12, December 1, 2007. ©ASCE, ISSN 1090-0241/2007/12-1512–1521/$25.00.

Table 1. Constitutive Model Parameters for the FE Analysis

Parameter	Aggregate	Alluvial clay	Desiccated fill
Effective stress friction angle, ϕ' (deg)	47	24	35
Effective stress cohesion, c' (kPa)	4	2	2
Dilatancy angle, ψ (deg)	12	0	0
Average wet density, γ (kg/m^3)	2,100	1,924	1,924
Deviatoric reference modulus, E_{50}^{ref} (kPa)	61,000	3,000	9,000
Compression reference modulus, E_{Oed}^{ref} (kPa)	61,000[a]	1,500	4,500
Unloading/reloading modulus, E_{ur}^{ref} (kPa)	1,220,000[b]	9,000[b]	27,000[b]
Power for stress-level dependency, m	0.48	1	1
Unloading/reloading Poisson's ratio, ν_{ur}	0.2	0.2	0.2
Reference stress, p^{ref} (kPa)	34.5	25.5	25.5
Failure ratio, R_f	0.88	0.96	0.96
K_0 for normal consolidation, K_0^{NC}	0.27	0.59	0.43
Initial void ratio, e_{ini}	0.33	1.0	1.0
Minimum void ratio (contraction), e_{min}	0.329	—	—
Maximum void ratio (dilation), e_{max}	0.393	—	—
Tensile cut-off, $\sigma_{tension}$	0	0	0

[a]Assume: $E_{Oed}^{ref}=E_{50}^{ref}$.
[b]Assume: $E_{ur}^{ref}=3E_{50}^{ref}$.

Descriptions of the FE Model

The finite element method has been previously used to model foundations supported by stone columns (Aboshi et al. 1979; Balaam and Brooker 1981; Mitchell and Huber 1985; Lee and Pande 1998; Kirsch and Sondermann 2001). In this study, an axisymmetric FE model was developed using the computer program Plaxis (version 8.2). The pier-supported footings were modeled as a unit cell which consists of a pier element supporting a circular footing. The tributary area of the unit cell was assumed to be one-fourth of the trial footing area. Details of the unit cell concept were described by Barksdale and Bachus (1983). Calculation of the tributary area based on pier spacing was suggested by Balaam and Brooker (1981). As will be shown later, this same model was used to study the response of isolated piers in which the diameter of the unit cell footing was equal to the pier diameter. Dimensions of the unit cell and the isolated pier in the models are shown in Fig. 1(a).

Fig. 1(b) shows the dimensions of the FE model used in this study. The model included a pier element installed in a two-layer matrix soil profile. The matrix soil profile consisted of a 1.0-m-thick desiccated layer overlying 13.0 m of soft alluvial soil. The physical boundary of the model was extended to 10.0 m measured radially from the center of the pier. The concrete in the footing was modeled as a linear elastic, nonporous material. Full fixity was provided along the bottom of the model. The vertical boundaries of the model were locked in the horizontal direction. An unstructured FE mesh that consists of 15-node, triangular elements was used. A fully drained condition was assumed for both pier installation and pier loading processes. A static pore water pressure profile was generated based on the location of the water table during testing which was set at 2.0 m from the ground surface. Measurements taken from piezometers installed near the piers edge at this site revealed that the excess pore water pressures dissipated within a few minutes after stopping the ramming operations (White et al. 2003).

Interface elements with strength reduction ratio of 0.5 were introduced along the footing-soil vertical interface to reflect a realistic contact condition between the footing and the soil. Thin solid continuum elements having effective shear strength parameters the same as those of the matrix soil were used along the pier-soil contact in lieu of interface elements (see Potts and Zdravkovic 1999).

Modeling Procedure

The initial condition was assumed to be at the end of the cavity drilling. Initial stresses were generated using the K_0 procedure in which the in situ effective horizontal stress was calculated as the product of the vertical effective stress and the predefined K_0 value. For the alluvial layer, $K_0=1-\sin\phi'$ was assumed, whereas $K_0=1.0$ was assigned to the desiccated layer. The initial shear stress was set to zero.

The pier installation process was modeled by applying outward uniform displacement along the shaft and downward uniform displacement at the bottom of the cavity. The strain-controlled cavity expansion process was terminated when the cavity strains along the shaft and at the bottom of the cavity were, respectively, equal to 5 and 10% of the nominal diameter of the cavity (Pham 2005). These cavity strain values were justified based on field measurements of the downward displacement after ramming the first lift of aggregate and diametric expansion measurements near the top of the cavity. The expanded cavity was filled with layers of compacted aggregate and the reinforced concrete footing was placed on top of the pier-soil system. The stress-controlled load tests were simulated by applying incremental to the top of the footing.

Model Verifications

Load-Deformation Behaviors

As previously described in Part I (White et al. 2007), two pier-supported footings (denoted as G_1 and G_2) and three isolated RAPs (denoted as P_1, P_2, and P_3) were constructed and tested at the same site. Verifications of the finite element model developed

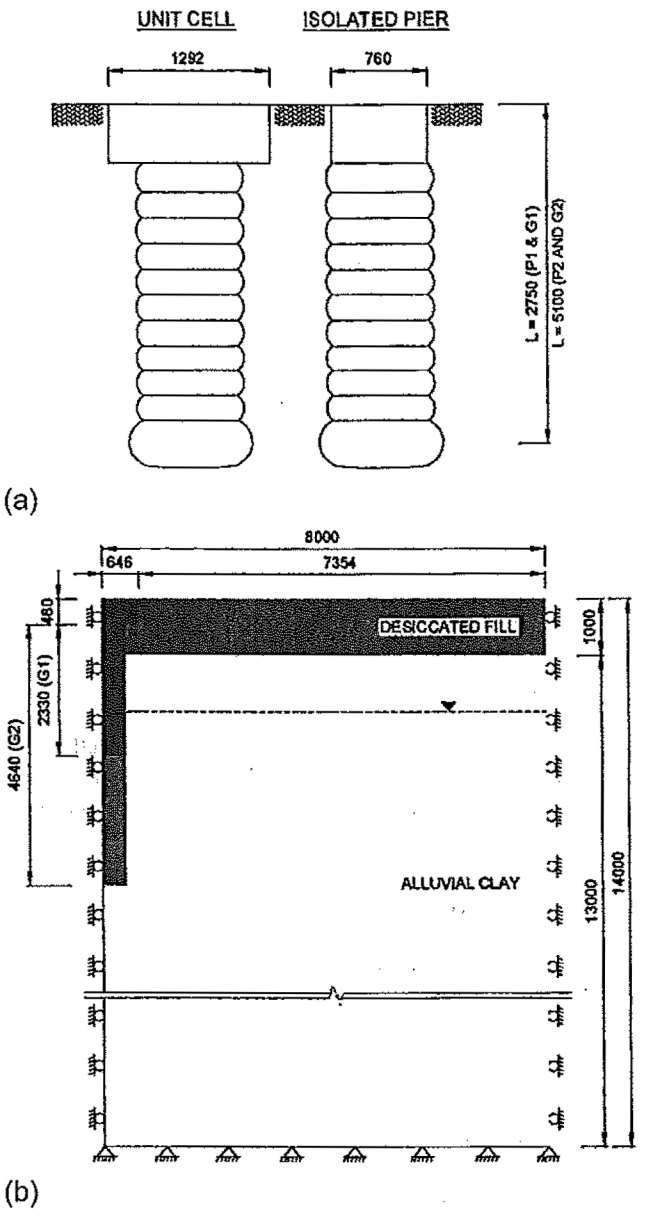

Fig. 1. (a) Dimensions of the unit cell and isolated pier; (b) the structural model of a unit cell (unit: mm)

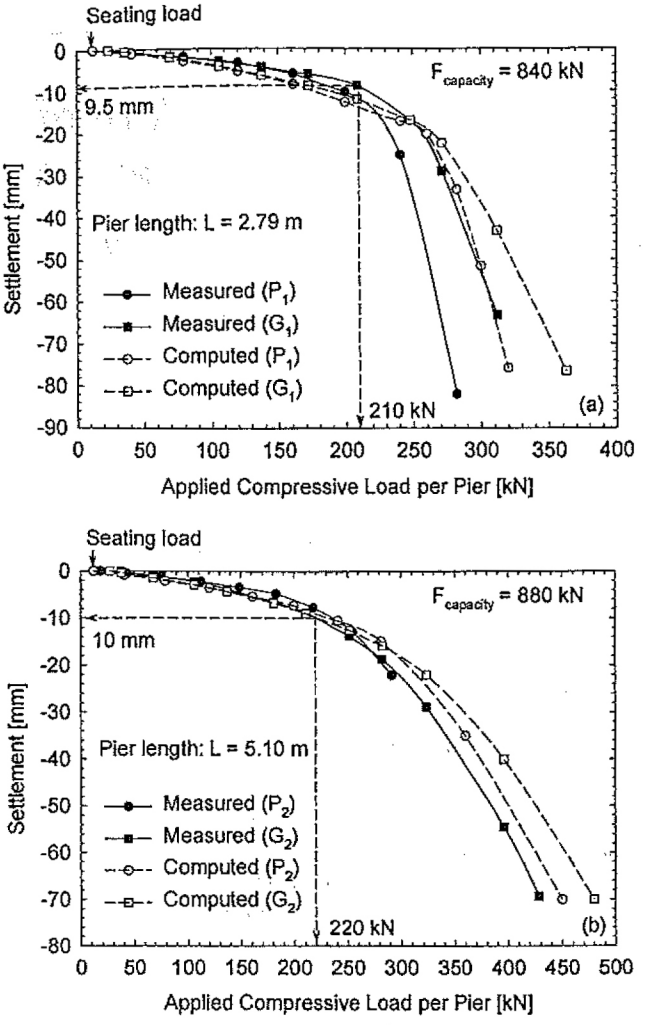

Fig. 2. Measurements versus FE computed values for load-settlement curves: (a) P_1 and G_1 and (b) P_2 and G_2. (Note: Total applied loads for footings G_1 and G_2 were divided by four for comparison to the isolated pier load test results.)

in this study are made by comparing the FE results with those measured from the full-scale, instrumented load tests conducted on both the pier-supported footings and the isolated piers. Fig. 2 compares the load-settlement curves computed from FE analyses with the measured curves from the full-scale load tests. The loads used to produce the load-settlement curves for G_1 and G_2 were calculated as one-fourth of the total applied load on the footing. In RAP design practice (Fox and Cowell 1998), the load capacity is commonly taken at the point of increased curvature of the load-settlement curve. Following this procedure, the load capacities of G_1 and G_2, as indicated in Fig. 2, are about 840 and 880 kN, respectively. As shown by Fig. 2, the computed load-settlement results agree well with the measurements until the compressive loads reach capacities. As the applied load exceeds this load level, FE analyses slightly underestimate the settlement. Finally, the load-settlement responses in both G_1 and G_2 are quite similar to those of the isolated piers with the same length and diameter.

Lateral Movement in the Matrix Soil

Fig. 3 shows the lateral displacement profile in the matrix soil adjacent to G_1 obtained from inclinometer measurements (casing 31 cm from edge of pier) and FE analyses. The maximum computed lateral displacements are 1.6 and 4.2 mm at compressive loads of 836 and 1,248 kN, respectively. Compared to measured displacements of 2.5 and 6.6 mm, the computed displacements are about 65% of the measured values. The depth of maximum deflection determined from the FE results is approximately 3.6 m, which is close to the measured value of about 3.4 m. Differences between the computed and the measured lateral displacements can be partly attributed to the incapability of the hardening-soil model in handling material anisotropy (i.e., different soil moduli in different directions).

Contact Stresses and Stress Concentration Ratio

Fig. 4 compares the total stress cell measurements and the computed contact stresses on top of the pier (q_g) and on top of the matrix soil (q_m) for G_1. Good agreement is achieved between the measured and the computed q_m. However, FE computed values slightly overestimate q_g for G_1. The computed stress concentra-

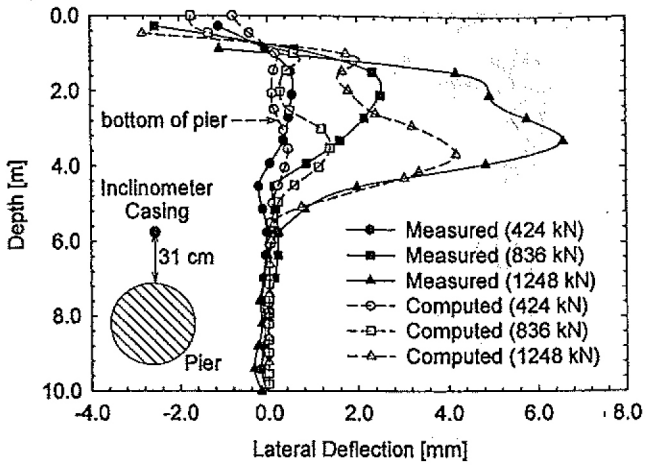

Fig. 3. Measurements versus FE computed values for lateral displacement in the matrix soil adjacent to G_1

tion ratio (R_s) values range from 2 to 10 for compressive loads of 143 to 1,085 kN, respectively. As shown in Fig. 4(b), R_s increases in G_1 with the compressive load up to a peak value (1,085 kN) before dropping to a somewhat constant value at higher loads. The drop and relatively constant R_s value at high compressive loads is attributed to both the pier and matrix soil reaching a failure stress state for which no additional load can be applied. Based on field measurements, Lawton and Warner (2004) also reported that R_s of a RAP-supported rigid footing decreased after the maximum design load is exceeded. A similar trending was

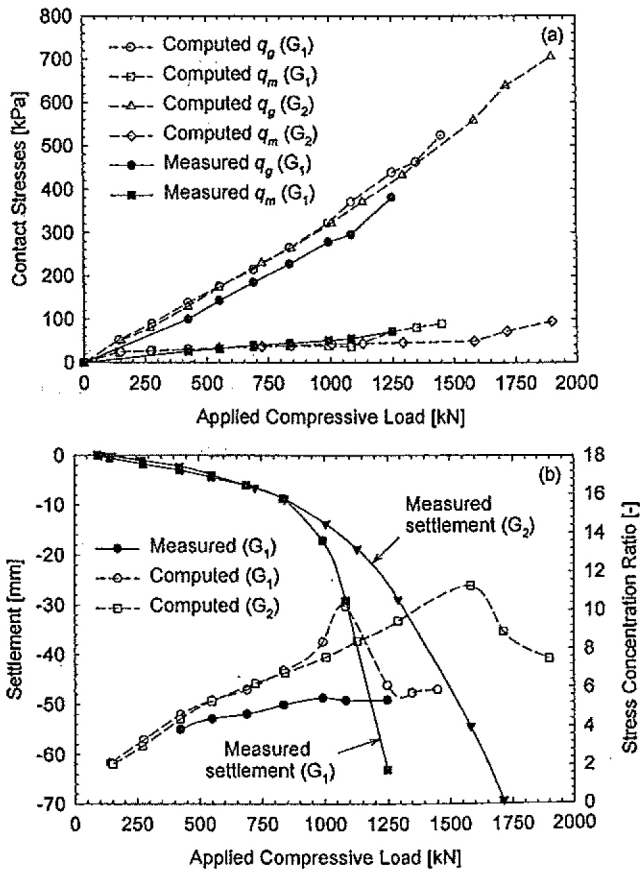

Fig. 4. Contact stress and stress concentration ratio for G_1 and G_2

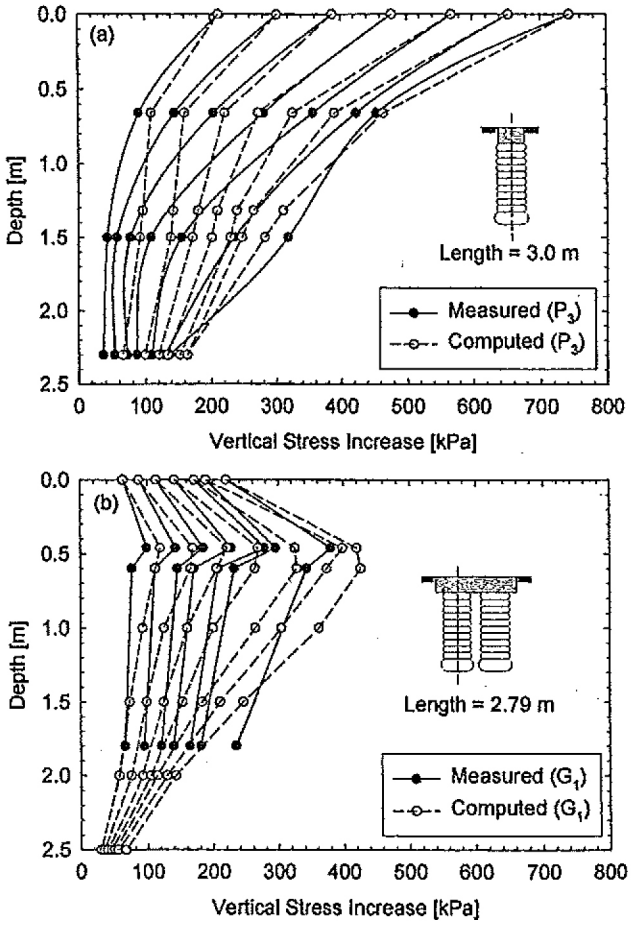

Fig. 5. Measurements versus FE computed values for stress distribution along pier shaft: (a) isolated pier (P_3); (b) pier group (G_1)

reported in Kirsch and Sondermann (2001) based on scaled model tests simulating stone columns. Also shown in Fig. 4 are q_g, q_m, and R_s values computed for G_2. When the applied compressive load is lower than about 800 kN, calculated q_g and q_m for both G_1 and G_2 are quite similar, except that a peak value of R_s of about 11 is achieved for G_2 at a compressive load of 1,584 kN.

Vertical Stress Distributions

Distributions of the vertical stress increase along the shaft of the isolated pier (P_3) and pier group (G_1) obtained from FE analyses and stress cell measurements are presented in Fig. 5. As indicated in Fig. 5(a), good agreement between the measured and the computed stresses in P_3 was attained especially at shallow depths and/or greater loads. Comparison of the measured and the computed stresses in G_1 [Fig. 5(b)] also showed good agreement, especially when considering the difficulties in accurately measuring total stress in the field (e.g., Dunnicliff 1993).

Comparison between Isolated Pier and Unit Cell Models

Although RAPs are commonly installed in groups, the settlement analysis of the pier group is essentially based on the behavior of an isolated pier (Fox and Cowell 1998). In this section, the response of a pier group modeled as a unit cell is compared with the

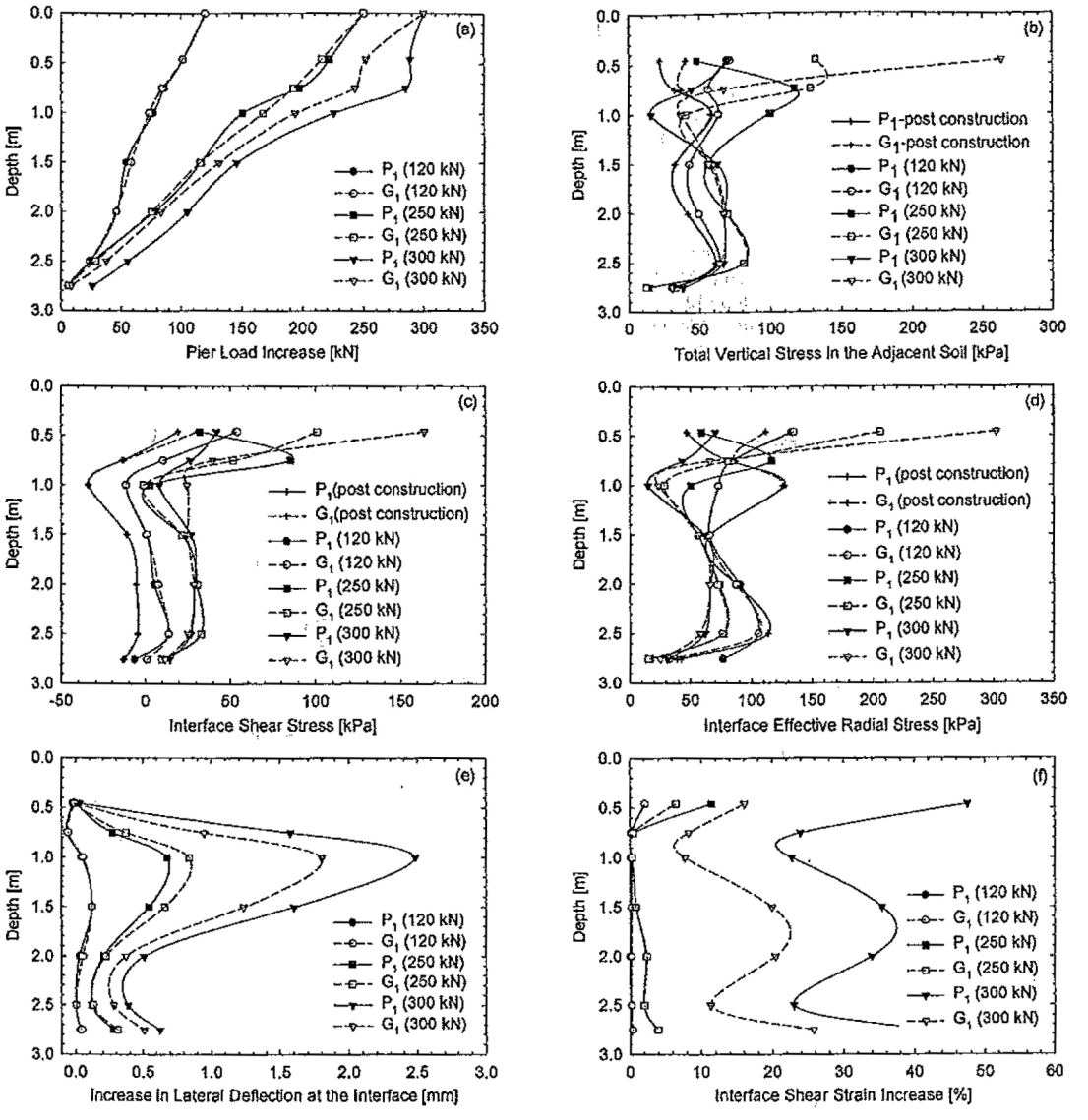

Fig. 6. Comparison of FE computed values between G_1 and P_1: (a) pier axial load increase; (b) vertical total stress in the matrix soil; (c) interface shear stress; (d) interface radial stress; (e) interface lateral deflection increase; and (f) interface shear strain increase

response of an isolated pier subjected to the same compressive loads.

Fig. 6 compares the behaviors of G_1 and P_1 by showing computed values for axial load distributions, vertical stresses in the matrix soil, interface shear stresses, lateral effective stresses in the matrix soil, lateral displacements in the matrix soil, and shear strains at the pier-soil contact. Three compressive loads (120, 250, and 300 kN) were selected for comparison. These loads correspond to less than capacity, capacity, and higher than capacity. As shown in Fig. 6(a), axial load distributions along P_1 and G_1 are almost coincident when the applied compressive load is less than or equal to 250 kN. This is because at these load levels, the differences in lateral effective stress [Fig. 6(d)] and interface shear strain [Fig. 6(f)] are small. When the applied compressive load is equal to 300 kN, the difference in both lateral effective stress and pier-soil interface shear strains becomes considerable between P_1 and G_1. The computed results show that the axial pier load dissipates more rapidly in G_1 compared to P_1 [Fig. 6(a)]. Further interpretation of the numerical results reveals that below a depth of about 1.0 m from grade, the distributions of all investigated parameters except the lateral displacement and the interface shear strain are similar between G_1 and P_1. Moreover, the increased lateral stress in G_1 due to the footing-induced vertical stress also prevents the lateral displacement in the matrix soil as shown in Fig. 6(e). At the load level (120 kN) less than capacity, the differences in the responses of G_1 and P_1 are insignificant.

Fig. 7 shows the comparison between P_2 and G_2. Similar to P_1 and G_1, three compressive loads of 120, 250, and 350 kN were selected for comparison. Above a depth of 1.0 m below grade, the vertical stress in the matrix soil [Fig. 7(b)], the lateral effective stress [Fig. 7(c)], and the interface shear stress [Fig. 7(d)] adjacent to G_2 are higher than those adjacent to P_2. At greater depths, all stresses are essentially the same in both cases. Compared to P_1 and G_1, the differences in all parameters between P_2 and G_2 are generally less. As a result, distributions of the axial pier load along G_2 and P_2 are quite similar even at compressive loads that exceed the load capacity (350 kN). Unlike P_1 and G_1, the interface shear strain in P_2 and G_2 is concentrated at the upper part of the pier, which is indicative of pier bulging.

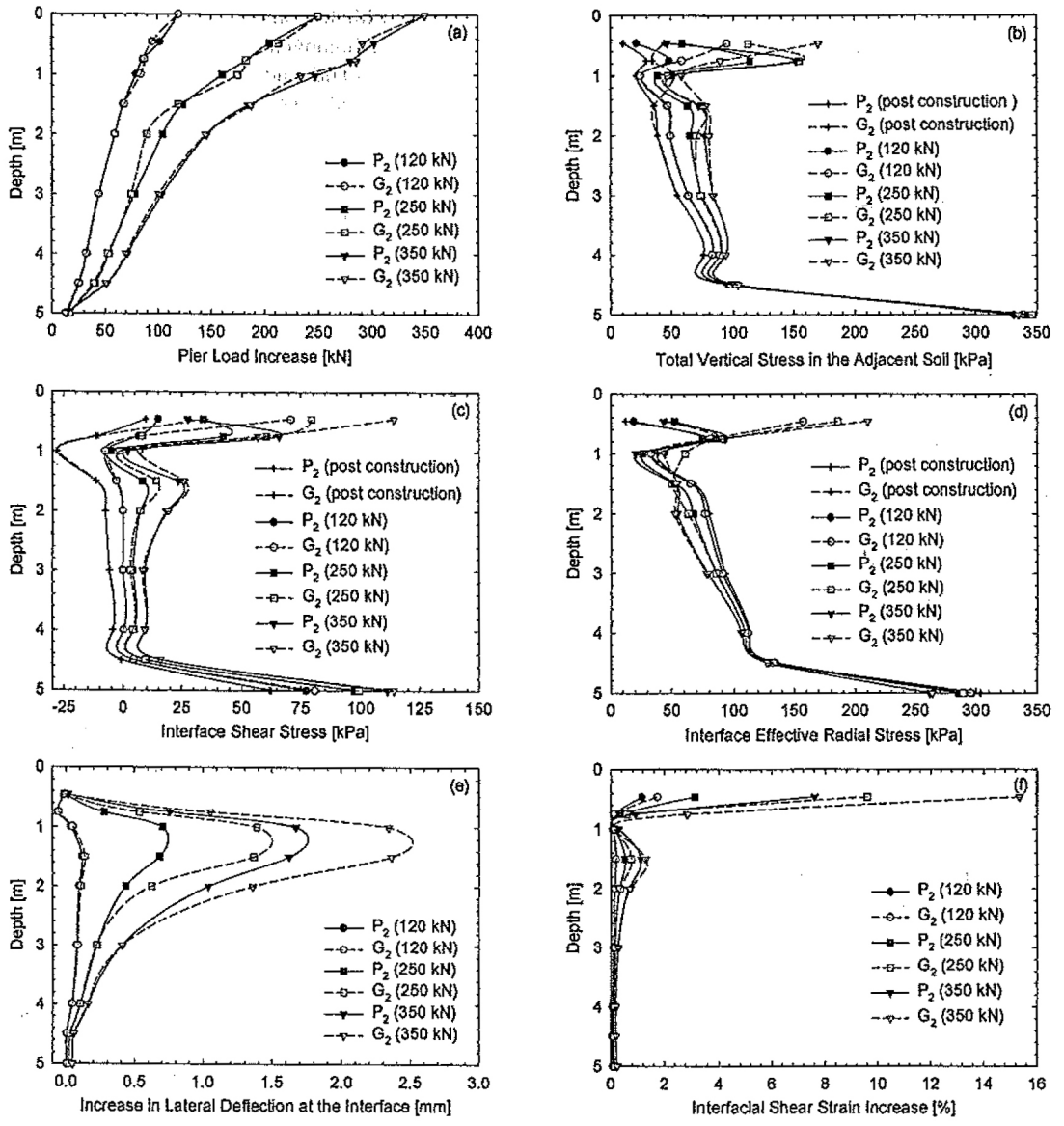

Fig. 7. Comparison of FE computed values between G_2 and P_2: (a) pier axial load increase; (b) vertical total stress increase in the matrix soil; (c) interface shear stress; (d) interface radial stress; (e) interface lateral deflection increase; and (f) interface shear strain increase

Stress Path in the Matrix Soil

To gain further insights into the pier-soil interactions, effective stress paths (following Lambe 1967) obtained from two soil elements adjacent to the unit cells (G_1 and G_2) and the isolated piers (P_1 and P_2) are shown in Fig. 8. These soil elements are arbitrarily located at 0.75 and 1.5 m below grade (0.29 and 1.04 m from footing bottom). Failure envelopes based on the friction angle of the alluvial clay (K_{f1}) and the desiccated layer (K_{f2}) are established in both compression and extension spaces. Stress states in both soil elements during cavity expansion were found to be on the extension failure envelopes, which indicate a Rankine passive stress condition. The application of compressive load on top of the pier during pier loading increases the shear stress in the soil elements and causes the stress paths to go upward into the compression space (i.e., above the p' axis). Once the Rankine active stress condition is reached, the stress path in the soil element located at 1.50 m continues to move upward along the failure envelope. However, the stress path in the soil element at 0.75 m declines along the failure envelope. This stress path direction indicates an unloading process. The stress paths of the soil elements at 1.50 m are similar between the unit cell and the isolated pier. For the soil elements 0.75 m, the stress path obtained from the unit cell is located to the right of stress path obtained from the isolated pier before reaching the Rankine active stress condition. This is because the vertical stress exerted from the unit cell footing increases the mean stress in the matrix soil.

In an axisymmetric analysis, there are four nonzero stress components: radial stress (σ'_r), vertical stress (σ'_z), tangential stress (σ'_θ), and the shear stress in the z-r plane (τ_{rz}). As other shear stresses ($\tau_{z\theta}$ and $\tau_{\theta r}$) are zero, the tangential stress, σ'_θ, is always one of the principal stresses. Depending on the loading condition, the tangential stress can either be the minor principal stress (σ'_3) or the intermediate principal stress (σ'_2). Principal stresses of two soil elements located at 0.75 and 1.50 m next to G_1 and G_2 are shown in Fig. 9 at different loading stages. Loading stages include the initial stress condition (initial), incremental

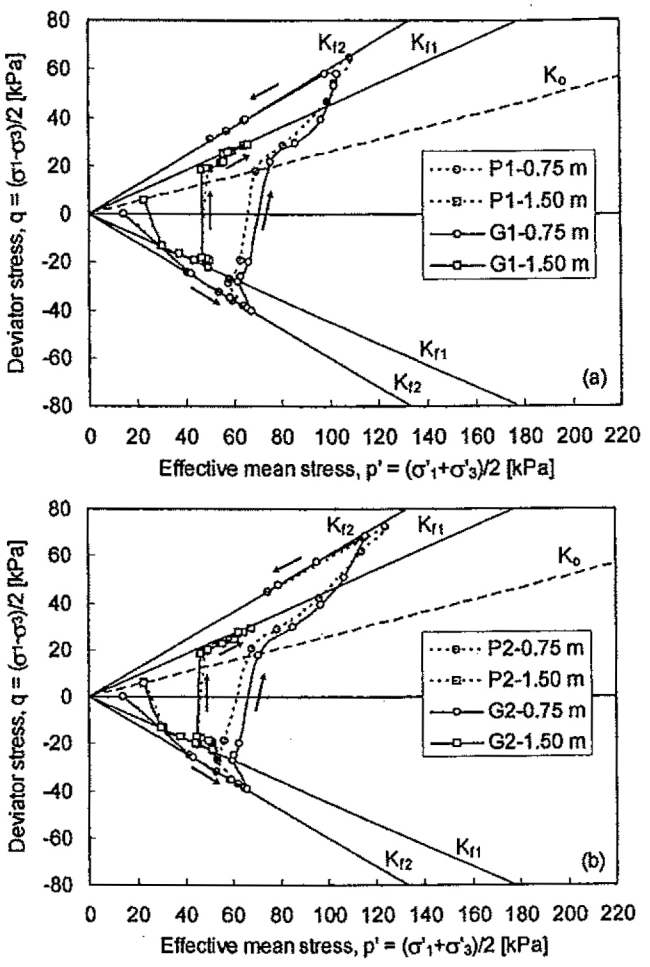

Fig. 8. Stress paths in the matrix soil adjacent to pier groups and single piers (a) P_1 and G_1; (b) P_2 and G_2

steps of cavity expansion during pier construction, and the application of vertical compressive loads. For the soil element at 1.50 m [Figs. 9(a and b)], the tangential stress in both G_1 and G_2 is always the minor principal stress. Therefore, for a given major principal stress (σ_1'), the tangential stress controls the magnitude of the deviator shear stress. On the other hand, the tangential stress is not always the minor principal stress in the soil element located at 0.75 m. As indicated in Figs. 9(c and d), the magnitude of the deviator stress is only controlled by the tangential stress when the applied compressive load is higher than 278 kN. At lower loads, the minor principal stress in the z-r plane controls the magnitude of deviator shear stress.

Stress Distribution underneath Pier-Supported Footings

Distributions of the vertical stress underneath footings supported by columnar systems are of practical importance. Knowledge of the stress distribution within the column-reinforced zone (i.e., upper zone) is necessary in estimating settlement and global stability (Barksdale and Bachus 1983). The characterization of the vertical stress distribution underneath a strip footing supported by end-bearing compacted sand columns using plain-strain FE analysis was conducted by Aboshi et al. (1979). In their analysis, vertical stress contours in the sand column-reinforced zone were compared with the stress contours obtained from Boussinesq's solution for a homogeneous, unreinforced soil. Following this approach, Barksdale and Bachus (1983) suggested a simplified method to estimate the vertical stress in the stone columns and the matrix soil by combining the Boussinesq's stress distribution with stress concentration ratio.

For floating systems such as RAPs, the distribution of vertical stress below the pier-reinforced zone (i.e., lower zone) is also needed for estimating the lower-zone settlement. Fig. 10 shows that the distribution of vertical stress underneath G_1 and G_2 can be estimated from the shaft length, H_{shaft}, using two linear functions with the following form:

$$\frac{\Delta\sigma_v}{q_0} = a - b\frac{z - D_f}{H_{shaft}} \tag{1}$$

where $\Delta\sigma_v$=vertical stress increase; q_0=applied footing pressure; z=depth below footing bottom; D_f=footing depth; and H_{shaft}=pier length. Values of a and b in Eq. (1) for the upper and the lower zone are shown in Fig. 10. As a conservative approach, current design practice for analyzing the settlement of RAP systems assumes that the vertical stress increase underneath the pier-supported footing follows the Westergaard's solution and that the stress distribution in both the upper and the lower zone is not affected by pier installation (Fox and Cowell 1998). Other analyses methods such as Schmertmann's layer strain approach, Boussinesq, and simple rules of 1.67 to 2.0 V:1.0H can also be used. In Fig. 10, the average vertical stress increase in G_1 and G_2 normalized by the applied footing pressure (q_0) is plotted against normalized depth. A hypothetical case which considers a footing constructed in an unreinforced soil is also analyzed using Westergaard's and FE solutions. Vertical stress distributions computed by these methods are compared with those determined by FE analyses when the footing is supported by G_1 and G_2. For the pier-reinforced cases, the average vertical stress is determined as the weighted average of the vertical stresses on top of the pier and on the matrix soil:

$$\Delta\sigma_v = \Delta q_g R_a + (1 - R_a)\Delta q_m \tag{2}$$

where $\Delta\sigma_v$=average vertical stress increase; Δq_g=vertical stress increase on the pier; Δq_m=vertical stress increase on the matrix soil; and R_a=area replacement ratio. As can be seen in Fig. 11, for the unreinforced case, $\Delta\sigma_v$ computed by the Westergaard's method is higher (conservative) compared to the FE solution. If the settlement induced by $\Delta\sigma_v$ is assumed to be terminated at the depth where $\Delta\sigma_v/q_o$ is 0.05, then the depths of zero settlement of G_1 and G_2 are equal to $1.5B$ and $2B$, respectively (where B is footing width). In other words, for a given footing width, the longer the pier, the deeper the vertical stress will be transmitted. As can be seen in Fig. 11, if the same assumption regarding the zero settlement depth is used for Westergaard's method then the settlement will be terminated at about $2.5B$. The sole dependence of $\Delta\sigma_v/q_0$ on the footing width when following Westergaard's solution can potentially cause inaccuracy in estimating stresses underneath pier-supported footings.

Summary and Conclusion

Numerical analyses using the FE method were conducted to study the mechanical behaviors of RAPs in supporting rigid footings. Group effects were investigated by comparing the behaviors of an individual pier in the group with those of an isolated pier of the

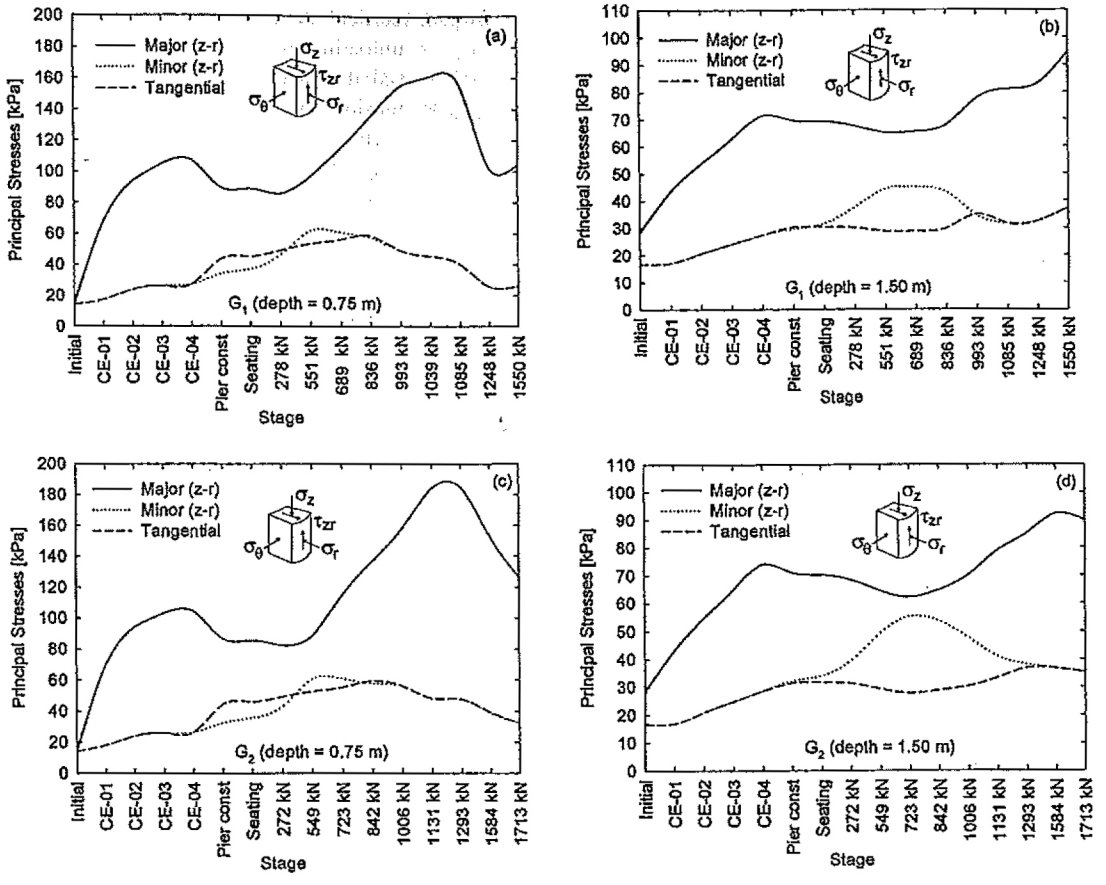

Fig. 9. Principal stresses in two soil elements adjacent to G_1 and G_2

same length and diameter. The numerical model developed in this study utilized model parameters that were estimated from in situ and laboratory tests. The FE model was verified by comparing the numerical results with those obtained from full scale compressive load tests with instrumentations. Conclusions drawn from this study are:

1. The FE model developed in this study successfully captured the mechanical behaviors of RAPs used to support rigid footings. The load-settlement response of a pier group can be computed from the modeling of an isolated pier of the same length and diameter. The stress concentration ratio was found to increase with the compressive load up to a peak level corresponding to the maximum design load. Continuing to increase the compressive load causes the stress concentration ratio to drop. This behavior was not observed in the field measurements.
2. Construction of the footing on top of the pier group increased the vertical stress in the matrix soil within the first meter from the footing bottom. As the vertical stress in the matrix

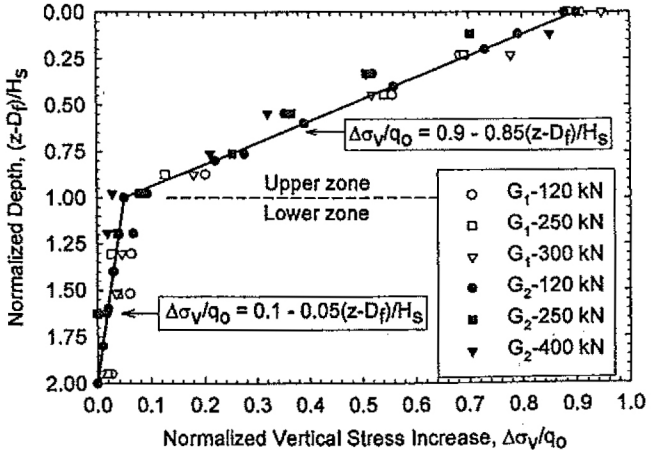

Fig. 10. Distribution of $\Delta\sigma_v$ below the footings as a function of shaft length

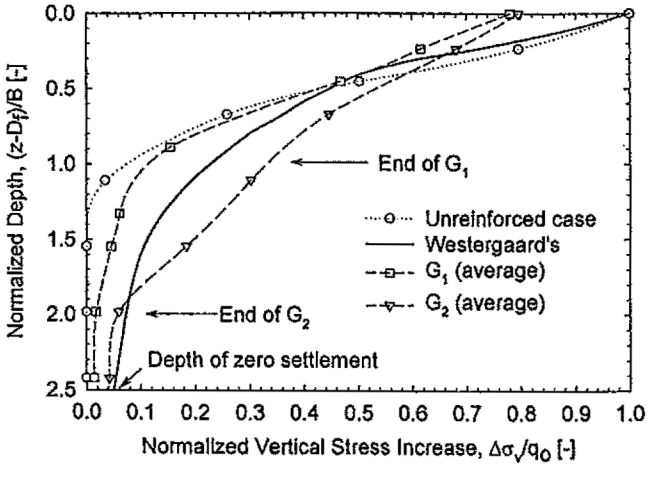

Fig. 11. Distribution of $\Delta\sigma_v$ below the footing as a function of footing width

soil increased, the lateral stress in the matrix soil also increased, thus promoting the development of pier-soil interface shear stress. However, it was found that the improvement in the pier-soil interface shear stress was not significant in this study. As a result, the behavior of the unit cell and the isolated pier are quite similar in terms of the distribution with depth of the axial pier load.

3. Analyses indicated that the Rankine passive stress condition was reached during pier installation. The application of compressive load on top of the pier during load tests increases the vertical stress in the soil elements and causes the stress paths to go upward toward the compressive failure envelope. The tangential stress only became the intermediate principal in the soil element located at 0.75 m when the compressive load was less than 278 kN.

- Using FE analyses, the vertical stress distribution in the upper and the lower zones underneath pier-supported footings can be characterized by two simple normalized linear functions.

Acknowledgments

This research was sponsored by the Geopier Foundation Company, Inc. and Iowa State University of Science and Technology. The support of these agencies is greatly acknowledged. Valuable comments and suggestions were provided by Dr. Kord Wissmann. The reviewers of this paper provided excellent reviews and very worthwhile suggestions.

Notation

The following symbols are used in this paper:

B = footing width;
c' = effective stress cohesion;
E_{comp} = elastic modulus of the pier-soil composite;
E_g = elastic modulus of the pier element;
e_{ini} = initial void ratio;
E_m = elastic modulus of matrix soil;
E_{ur}^{ref} = reference unloading/reloading modulus corresponding to p^{ref};
E_{0ed}^{ref} = reference modulus corresponding to p^{ref};
E_{50}^{ref} = reference secant modulus corresponding to p^{ref};
e_{max} = maximum void ratio;
e_{min} = minimum void ratio;
K_f = slope of the failure envelope in p-q space;
K_0 = *at-rest* coefficient of lateral earth pressure;
m = power for stress-level dependency;
p^{ref} = reference confining stress;
p' = mean effective stress;
q_g = stress concentrated on top of the pier element;
q_m = stress concentrated on top of matrix soil;
q_0 = induced pressure at the footing bottom;
R_a = area replacement ratio;
R_f = failure ratio;
R_s = stress concentration ratio;
S_{UZ} = settlement of the upper zone;
γ = wet density;
Δq_g = increase in the stress on top of the pier element;
Δq_m = increase in the stress on top of matrix soil;
$\Delta\sigma_v$ = vertical stress increase due to footing pressure;
ν_{ur} = unloading-reloading Poisson's ratio;
σ_r' = radial effective stress;
$\sigma_{tension}$ = tension cut-off stress;
σ_z' = vertical effective stress;
σ_θ' = tangential effective stress;
σ_1' = major principal effective stress;
σ_3' = minor principal effective stress;
τ_{rz} = shear stress in z-r plan;
ϕ' = effective stress friction angle; and
ψ = dilatancy angle.

References

Aboshi, H., Ichimoto, E., Enoki, M., and Harada, K. (1979). "The compozer: A method to improve characteristics of soft clays by inclusions of large diameter sand columns." *Proc., Int. Conf. on Soil Reinforcement: Reinforced Earth and Other Techniques*, Vol. 1, Paris, 211–216.

Balaam, N. P., and Brooker, J. R. (1981). "Analysis of rigid rafts supported by granular piles." *Int. J. Numer. Analyt. Meth. Geomech.*, 5(4), 379–403.

Barksdale, R. D., and Bachus, R. C. (1983). "Design and construction of stone columns." *Rep. No. FHWA/RD-83/026*, National Technical Information Service, Springfield, Va.

Dunnicliff, J. (1993). *Geotechnical instrumentation for monitoring field performance*, Wiley, New York.

Fox, N. S., and Cowell, M. J. (1998). *Geopier™ foundation and soil reinforcement manual*, Geopier Foundation, Blacksburg, Va.

Handy, R. L., Fox, N. S., and Wissmann, K. J. (1999). "Short aggregate piers reinforce soils near tunnels." *Proc., Geo-Engineering for Underground Facilities, Geotechnical Special Publication No. 90*, ASCE, Reston, Va., 1039–1047.

Kirsch, F., and Sondermann, W. (2001). "Ground improvement and its numerical analysis." *Proc., 15th Int. Conf. on Soil Mechanics and Foundation Engineering*, ISSMGE, Istanbul, Turkey, 1775–1778.

Lambe, T. (1967). "The stress-path methods." *ASCE:JSMFD*, 93(6), 309–331.

Lawton, E. C., and Fox, N. S. (1994). "Settlement of structures supported on marginal or inadequate soils stiffened with short aggregate piers." *Proc. Vertical and Horizontal Deformations of Foundations and Embankments, Geotechnical Special Publication No. 40*, ASCE, College Station, Tex., Vol. 2, 962–974.

Lawton, E. C., Fox, N. S., and Handy, R. L. (1994). "Control of settlement and uplift structures using short aggregate piers." *Proc., In-Situ Deep Soil Improvement, Geotechnical Special Publication No. 45*, ASCE, Atlanta, 121–132.

Lawton, E. C., and Warner, B. J. (2004). "Performance of a group of Geopier elements loaded in compression compared to single Geopier elements and unreinforced soil." *Final Rep., Rep. No. UUCVEEN 04-12*, Univ. of Utah, Salt Lake City.

Lee, J. S., and Pande, G. N. (1998). "Analysis of stone-column reinforced foundations." *Int. J. Numer. Analyt. Meth. Geomech.*, 22(12), 1001–1020.

Mitchell, J. K., and Huber, T. R. (1985). "Performance of stone column foundation." *J. Geotech. Engrg.*, 111(2), 205–223.

Pham, H. (2005). "Support mechanism for rammed aggregate piers." Ph.D. Dissertation, Iowa State University, Ames, Iowa.

Potts, D. M., and Zdravkovic, L. (1999). *Finite element analysis in geotechnical engineering: Vol. I—Theory*, Telford, London.

Schanz, T., Vermeer, P. A., and Bonnier, P. G. (1999). "Formulation and verification of the hardening-soil model." *Proc., Beyond 2000 in Computational Geotechnics*, Balkema, Rotterdam, The Netherlands, 281–290.

White, D. J., Gaul, A. J., and Hoevelkamp, K. (2003). "Highway appli-

cations for rammed aggregate pier in Iowa soils." *Final Rep., DOT TR-443*, Ames, Iowa.

White, D. J., Pham, H. T. V., and Hoevelkamp, K. K. (2007). "Support mechanisms of rammed aggregate piers. I: Experimental results." *J. Geotech. Geoenviron. Eng.*, 133(12), 1503–1511.

White, D. J., Suleiman, M. T., Pham, H. T., and Bigelow, J. (2002). "Constitutive equations for aggregates used in Geopier® foundation construction. *Final Rep.*, Iowa State Univ., Ames, Iowa.

Wissmann, K. J., Moser, K., and Pando, M. (2001). "Reducing settlement risks in residual piedmont soil using rammed aggregate pier elements." *Proc., Foundations and Ground Improvement, Geotechnical Special Publication No. 113*, ASCE, Blacksburg, Va, 943–957.

contents continued from front cover

ASCE
American Society of Civil Engineers
1801 Alexander Bell Drive
RESTON, VA 20191-4400